Substitutional alloy of Ce and Al

Qiao-Shi Zeng[a,b], Yang Ding[b], Wendy L. Mao[c,d], Wei Luo[e,f], Andreas Blomqvist[e], Rajeev Ahuja[e,f], Wenge Yang[g], Jinfu Shu[h], Stas V. Sinogeikin[g], Yue Meng[g], Dale L. Brewe[i], Jian-Zhong Jiang[a,1], and Ho-kwang Mao[a,b,g,h,1]

[a]International Center for New-Structured Materials, and Laboratory of New-Structured Materials, Department of Materials Science and Engineering, Zhejiang University, Hangzhou 310027, China; [b]High Pressure Synergetic Consortium and [g]High Pressure Collaborative Access Team, Carnegie Institution of Washington, Argonne, IL 60439; [c]Department of Geological and Environmental Sciences, Stanford University, Stanford, CA 94305; [d]Photon Science Department, SLAC National Accelerator Center, Menlo Park, CA 94025; [e]Condensed Matter Theory Group, Department of Physics, Uppsala University, Box 530, SE-751 21 Uppsala, Sweden; [f]Department of Materials Science and Engineering, Royal Institute of Technology, SE-100 44 Stockholm, Sweden; [h]Geophysical Laboratory, Carnegie Institution of Washington, Washington, DC 20015; and [i]Pacific Northwest Consortium Collaborative Access Team/X-ray Operations and Research, Advanced Photon Source, Argonne National Laboratory, Argonne, IL 60439

Contributed by Ho-kwang Mao, December 30, 2008 (sent for review November 30, 2008)

The formation of substitutional alloys has been restricted to elements with similar atomic radii and electronegativity. Using high-pressure at 298 K, we synthesized a face-centered cubic disordered alloy of highly dissimilar elements (large Ce and small Al atoms) by compressing the Ce_3Al intermetallic compound >15 GPa or the Ce_3Al metallic glass >25 GPa. Synchrotron X-ray diffraction, Ce L_3-edge absorption spectroscopy, and ab initio calculations revealed that the pressure-induced Kondo volume collapse and 4*f* electron delocalization of Ce reduced the differences between Ce and Al and brought them within the Hume-Rothery (HR) limit for substitutional alloying. The alloy remained after complete release of pressure, which was also accompanied by the transformation of Ce back to its ambient 4*f* electron localized state and reversal of the Kondo volume collapse, resulting in a non-HR alloy at ambient conditions.

4*f* electron delocalization | Ce-Al solid solution alloy | high pressure | Hume-Rothery rules | metallic glass

Combining one metal with another leads to a range of alloys with properties superior to each individual end member. Since the Bronze and Iron Ages, the quest for new metallic alloys through various chemical and metastable quenching paths has played a crucial role in the advancement of civilizations. The most common type of alloy is a substitutional crystalline solid solution in which atoms of one element randomly substitute for atoms of another element in a crystal structure. The possibilities for substitution, however, are restricted by the classic empirical Hume-Rothery (HR) rules (1), which require the components have atomic size within 15% and electronegativity within 0.4 of each other. For instance, the archetypal 4*f* metal Ce alloys with similar rare-earth metals to form "mischmetal," which has unusual pyrophoric properties and strength for a broad range of chemical and physical applications, and the *sp*-bonded light metal Al alloys with similar atoms to form a family of aluminum alloys that have enormous technological importance and application in everyday life. No known binary substitutional crystalline alloy exists between Ce and Al because their differences of 28% in atomic radii and 0.45 in electronegativity far exceed the HR limit. They can only form stoichiometric compounds in which Ce and Al are chemically ordered and occupy separate crystallographic sites, or metallic glass synthesized by rapidly quenched from melt in which Ce and Al are disordered both chemically and structurally. Here, we report the formation of a Ce-Al substitutional crystalline alloy from intermetallic compound and metallic glass at high pressure and room temperature, this alloy can be recovered as a non-HR alloy to ambient conditions.

Pressure is a powerful tool for altering individual atoms and their electronic structures, changing the bonding chemistry, and creating novel materials (see, for example, ref. 2). This has been demonstrated by the discovery of intermetallic compounds in the incompatible K-Ni and K-Ag systems under high pressures and temperatures (3–5). These novel materials, however, are not quenchable. Pressure and temperature have been used to increase the solubility of small Mg atoms in an alloy with large Fe atoms up to 4 at. % (atomic percent) at 20 GPa and 2,470 K and up to 10 at. % at 126 GPa and 3,650 K (6). The dissimilarity between Mg and Fe was reduced gradually by the differential compressibility of Mg and Fe. Extreme pressures and temperatures are required to accomplish even a modest solubility.

Pressure has been known to induce drastic changes in Ce (7–9) at low temperatures. Above 0.8 GPa at 298 K, pure Ce metal undergoes an isostructural transition from an a face-centered cubic (fcc) phase (γ-Ce) to a denser, high-pressure, fcc phase (α-Ce) accompanied by a 15% volume collapse. Since its discovery by P. W. Bridgman in 1927 (10), the γ-α Ce transition has been the subject of extensive experimental (11, 12) and theoretical investigations (7, 13–16) and is often cited as an archetypal example of a localized-itinerant 4*f* electronic transition. Various scenarios including Mott transition (7), Kondo hybridization (8, 13), and intermediate behaviors between the two (14, 15) have been proposed. Regardless of the scenario, the phenomenological volume collapse in Ce atoms would certainly be helpful in reducing the difference in atomic size between the large Ce and small Al atoms and could aid our efforts toward overcoming the HR limitations.

Results and Discussion

Metallic glass quenched from rapid cooling of melt is an interesting new type of amorphous material with a densely packed structure (17). Structures and polyamorphic transitions of Ce-Al metallic glasses have recently received increasing attention (18–21). We studied X-ray diffraction (XRD) of a metallic glass with the Ce_3Al composition under hydrostatic pressures in helium medium and room temperature (see *Materials and Methods* for details). Results are presented in Fig. 1*A*. The sample remained a metallic glass and showed the characteristic broad amorphous XRD features up to 24.4 GPa. At 25.0 GPa, the amorphous XRD pattern vanished and sharp crystalline peaks suddenly appeared, indicating the observation of hydrostatic pressure-induced full crystallization of metallic glass at room temperature. Although pressure-induced crystallization of ordinary amorphous materials at low temperatures has been well established (22, 23), previous reports of pressure-induced crystallization of metallic glass are either on samples that are highly strained (24) or of uncertain crystallinity and structure (25). The present XRD pattern of the crystallized metallic glass fits an fcc crystal structure. The new fcc phase remained as the sample was gradually decompressed back to ambient pressure.

Ce and Al also form a series of stoichiometric compounds (Ce_xAl_y with integer x and y) exhibiting interesting magnetic order-

Author contributions: J.-Z.J. and H.-k.M. designed research; Q.-S.Z., Y.D., W.Y., J.S., S.V.S., Y.M., and D.L.B. performed research; Q.-S.Z., J.-Z.J., and H.-k.M. contributed new reagents/analytic tools; Q.-S.Z., Y.D., W.L.M., W.L., A.B., R.A., W.Y., J.-Z.J., and H.-k.M. analyzed data; and Q.-S.Z., Y.D., W.L.M., J.-Z.J., and H.-k.M. wrote the paper.

The authors declare no conflict of interest.

[1]To whom correspondence may be addressed. E-mail: jiangjz@zju.edu.cn or hmao@gl.ciw.edu.

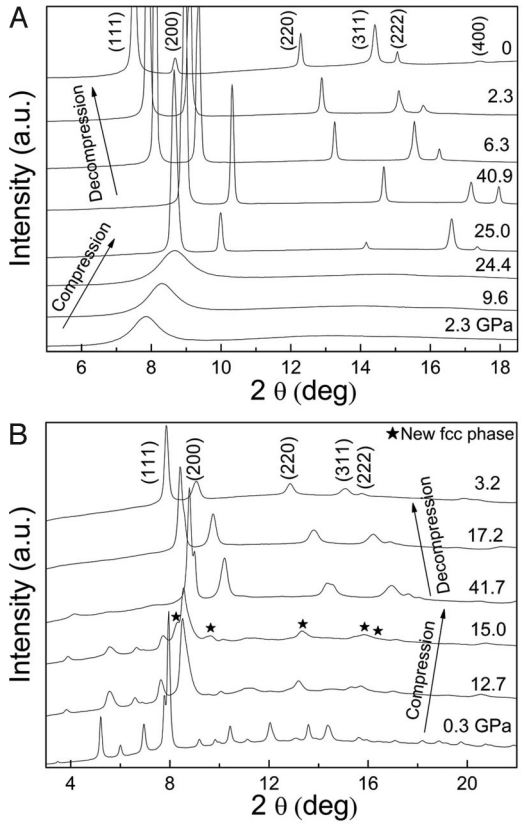

Fig. 1. XRD patterns of Ce_3Al at high pressures and 298 K using X-ray wavelength $\lambda = 0.3681(1)$ Å. (*A*) Starting with a metallic glass, the transition occurs at 25 GPa. Intensity mismatch to the fcc structure is caused by the growth of large crystals in our sample. (*B*) Starting with hexagonal α-Ce_3Al, the transition occurs at 15 GPa.

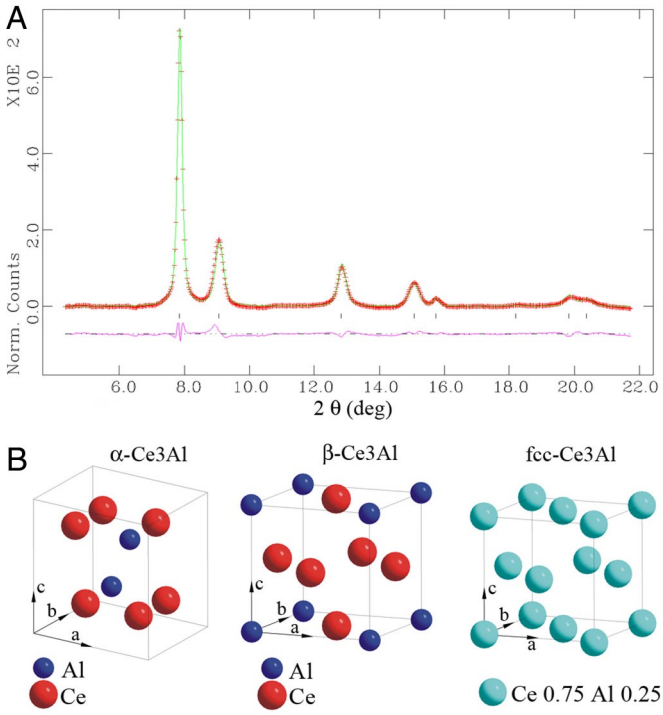

Fig. 2. Atomic structure models of Ce-Al alloy. (*A*) Rietveld refinement of the new fcc phase at 3.2 GPa synthesized from polycrystalline α-Ce_3Al (wRp = 0.86%, Rp = 0.59%, $a = 4.6494 \pm 0.0002$ Å). The refinement indicates the atoms at the 4 equivalent *Fm3m* lattice points are indistinguishable, i.e., the fcc phase is a substitutional, solid-solution alloy of Ce_3Al with the Ce occupancy of 0.75 and Al occupancy of 0.25 at lattice points (0, 0, 0), (0,0.5,0.5), (0.5,0.5,0), (0.5,0,0.5). (*B*) Crystal structures of the 2 ordered compounds α-Ce_3Al and β-Ce_3Al and the disordered fcc-Ce_3Al alloy.

ing and Kondo behavior (26). At ambient pressure and temperature, the compound Ce_3Al crystallizes in the form of hexagonal α-Ce_3Al (space group $P6_3/mmc$) (27). We studied XRD of α-Ce_3Al under quasi-hydrostatic pressures in silicon oil medium; the results are shown in Fig. 1*B*. Below 12.7 GPa, only the α-Ce_3Al XRD pattern was present. Above 15 GPa, an fcc phase similar to the product from compression of the metallic glass appeared, and the new alloy grew at the expense of the α-Ce_3Al phase with further pressure increase. Therefore, we have confirmed that the fcc alloy was the final high-pressure product with both starting materials and was quenchable in both experiments. Compared with the metallic glass experiment, the α-Ce_3Al experiment has broader XRD peaks, a lower starting transition pressure to the fcc alloy, a larger hysteresis 2-phase range, and a larger zero-pressure volume of the final fcc alloy (Fig. 1 and Table 1). The difference could be attributed to the different starting materials and different degrees of strain and nonhydrostaticity of the helium and silicon oil pressure media.

All XRD peaks from the new phase can be indexed to an fcc unit cell (Table 1 and Fig. 2). This cubic phase strictly follows the extinction rules for space group *Fm3m* (i.e., only all-even or all-odd *hkl* reflections are allowed), and is different from the high-temperature simple cubic phase, the chemically-ordered β-Ce_3Al with space group *Pm3m*. This small fcc unit cell can only accommodate a single atom at the *Fm3m* lattice point (Z = 4). Ce and Al atoms must be disordered to share the single point randomly, i.e.,

Table 1. Unit-cell dimension (*a*) and *d*-spacings of the Ce_3Al fcc alloy at different pressures during decompression after its high-pressure, room-temperature synthesis from the metallic glass Ce_3Al and intermetallic compound α-Ce_3Al starting materials

	Metallic glass				α-Ce_3Al			
	hkl				*hkl*			
Dimension/ spacing	d_{cal}, Å	d_{obs}, Å	d_{cal},Å	d_{obs}, Å	d_{cal}, Å	d_{obs}, Å	d_{cal}, Å	d_{obs}, Å
111	2.8096	2.8099	2.6038	2.6038	2.8234	2.8205	2.6844	2.6841
200	2.4332	2.4311	2.2550	2.2581	2.4451	2.4538	2.3247	2.3312
220	1.7205	1.7202	1.5945	1.5943	1.7290	1.7287	1.6438	1.6439
311	1.4672	1.4672	1.3598	1.3609	1.4745	1.4732	1.4019	1.4031
222	1.4048	1.4049	1.3019	1.3016	1.4117	1.4095	1.3422	1.3426
P, GPa	0.0		6.2		0.0		3.2	
a, Å	4.8662(3)		4.5099(4)		4.8902(3)		4.6494(2)	

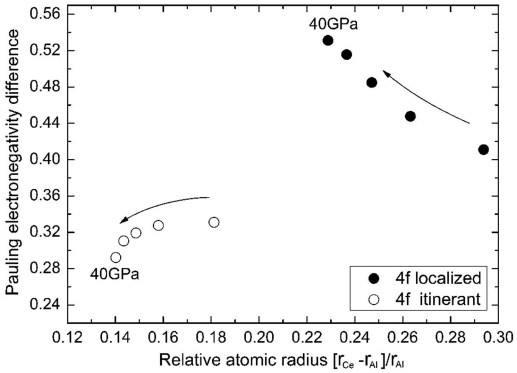

Fig. 3. Darken-Gurry map of Ce in reference to Al calculated from theory. Results for pressures of 0, 10, 20, 30, and 40 GPa are shown by circles (4*f* electron localized, filled; itinerant, open). Arrows indicate the direction of increasing pressure.

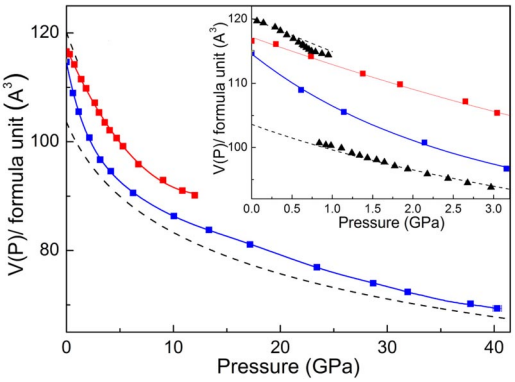

Fig. 4. *P-V* relations for Ce_3Al up to 40 GPa. The high-pressure volumes of α-Ce_3Al (red squares) and fcc alloy (blue squares) were determined in the present study by in situ XRD during pressure increase and release. The dashed curves are ($3V_{\gamma\text{-}Ce} + V_{Al}$) and ($3V_{\alpha\text{-}Ce} + V_{Al}$) at pressures $<$ and $>$1 GPa, respectively, calculated by using results from the volumes for pure Ce (V_{Ce}) (29) and pure Al (V_{Al}) (30). (*Inset*) Expanded *P-V* plot up to 3 GPa; recent high-precision data of V_{Ce} from ref. 28 were used to calculate the black triangles.

they form a substitutional, solid-solution crystalline alloy of Ce_3Al (Fig. 2). The fcc Ce_3Al alloy was preserved after complete decompression to ambient pressure at 298–420 K and has remained structurally and chemically unchanged without evidence of oxidation or deterioration in air during the past 12 months.

The irreversibility of the transition implies metastability and a true equilibrium transition pressure between 0 and 15 GPa. To overcome the kinetic barrier for synthesis, we carried out another experiment using a double-sided Nd:YLF laser system to heat the α-Ce_3Al sample in situ at high pressures to moderate temperatures ($<$900 K). Reversible transitions between the hexagonal α-Ce_3Al and the new fcc alloy were observed between 5 and 6 GPa during heating, thus further narrowing down the equilibrium transition pressure. The moderate pressure-temperature synthesis conditions and the long-term metastability of the fcc alloy enhance the possibility of developing this alloy for practical applications.

The surprising discovery of the fcc-Ce_3Al substitutional alloy may be understood considering the pressure effect on Ce. We conducted ab initio theoretical calculations for the atomic radii and electronegativity of both 4*f* electron localized and itinerant Ce in the fcc-Ce_3Al alloy. The results are shown in the empirical Darken-Gurry map using the Al atom as the reference (Fig. 3). At ambient pressure and temperature, the 4*f* localized Ce is clearly too different from Al in terms of both atomic size and electronegativity, thus preventing the alloying with Al. The larger compressibility of Ce compared with Al allows pressure to narrow the size difference between 4*f* electron localized Ce and Al, but the difference is still as large as 22% up to 40 GPa. In addition, pressure widens the difference in electronegativity between Al and 4*f* electron localized Ce and reduces the likelihood of forming a substitutional alloy. However, 4*f* itinerant Ce has a much smaller radii that is within 18% of Al at zero pressure, and the differential compressibility between Ce and Al further reduces the difference to 15% at 20 GPa. In addition, the electronegativity of 4*f* electron itinerant Ce is much closer to Al and the negative pressure dependence brings them into even better agreement. Overall, the pressure-induced 4*f* electronic delocalization transition brings Ce and Al into compliance with the HR rules for the formation of the fcc alloy.

During pressure release, the 4*f* itinerant-localization electronic transition only involves the movement of electrons and is readily reversible, whereas the Ce-Al disorder–order structural transition requires the movement of atoms and is much more sluggish, thus locking in the non-HR alloy. Although our theoretical calculations do not provide information on reaction kinetics, our experiments show that the disordered fcc alloy remains crystalline instead of reversal to an ordered α-Ce_3Al phase or a totally disordered amorphous phase at zero pressure, indicating that the expansion of Ce atoms during the reversal 4*f* electronic transition has not reached the Lindemann lattice instability criterion. At zero pressure $>$430 K, we observed the growth of additional cubic peaks that are forbidden in *Fm3m* but allowed in the *Pm3m* space group, indicating the ordering of Ce and Al atoms in the crystal.

The above scenario was confirmed by the results of synchrotron XRD and X-ray absorption spectroscopy (XAS). In Fig. 4, the volume of the fcc-Ce_3Al alloy determined by in situ XRD is compared with that of α-Ce_3Al and 3:1 mixture of pure Ce and Al (9, 28–30). At increasing pressures after the synthesis of the fcc alloy, its volume asymptotically approaches ($3V_{\alpha\text{-}Ce} + V_{Al}$) within 2% at high pressures, indicating the Kondo volume collapse of Ce in the fcc alloy. When pressure is released $<$3 GPa, the Fig. 4 *Inset*

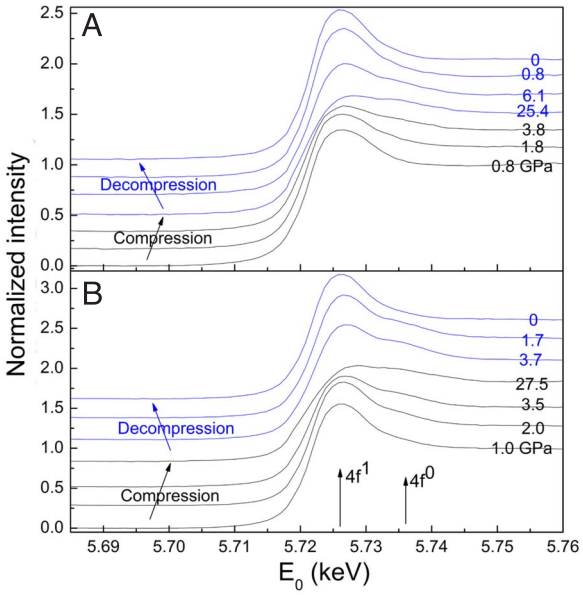

Fig. 5. In situ XAS spectra of Ce L_3-edge with α-Ce_3Al compound (*A*) and Ce_3Al metallic glass (*B*) as the starting materials. Starting phases during compression (black curves), and fcc alloy after conversion and during decompression (blue curves) are shown. The numbers on each pattern denote the pressures, and the arrows point to the $4f^0$ and $4f^1$ components. The appearance of the $4f^0$ feature indicates the delocalization of 4*f* electron, which coincides with the relatively sharp drop in pressure dependence observed in Ce_3Al volume in Fig. 4.

shows that the volume of the fcc alloy expands rapidly and approaches that of the $V_{\alpha\text{-}Ce3Al}$ and $(3V_{\gamma\text{-}Ce} + V_{Al})$ at zero pressure, indicating the reversal of the Kondo volume collapse of Ce in the fcc alloy.

The XAS of Ce L_3-edge was measured as a function of pressure and is presented in Fig. 5. During compression, the postedge feature denoted $4f^0$ (12, 31) clearly grows with increasing pressure and transition to fcc-Ce_3Al. After decompression, the $4f^0$ feature vanishes and the original $4f^1$ feature returns, indicating that the quenched fcc-Ce_3Al is a non-HR alloy with large differences in atomic size and electronic properties between Ce and Al. Because the volume expansion and $4f$ electron localization is a continuous process, we cannot rule out the possibility of incomplete reversal.

Conclusions

Pressure induces Kondo volume collapse and delocalization of the $4f$ electrons of Ce that brings Ce and Al into compliance with the HR rules for the formation of the substitutional fcc alloy. The electronic transition is reversible, whereas the structure transition is irreversible. The present discovery opens an additional route for making novel alloys including Ce-Al alloys of ratios other than 3:1, Ce alloys with other incompatible elements, and other f-electron alloys. Such alloys may display a range of unusual and useful mechanical, electronic, and magnetic properties and greatly increase the choice of materials for a variety of applications.

Materials and Methods

Ce_3Al metallic glass ribbons of 15-μm thickness and 1-mm width were prepared by using the single-roller, melt-spinning method. Hexagonal intermetallic compound α-Ce_3Al was synthesized by annealing the Ce_3Al metallic glass ribbons at 200°C in silicon oil for 1 day. After removing the oxidized surface layer, the sample was confirmed by XRD to be a single phase of polycrystalline α-Ce_3Al. The samples were cut into $50 \times 50 \times 12$-μm^3 pieces, and loaded in a Mao-type symmetric diamond anvil cell (DAC) along with a tiny chip of ruby as the pressure calibrant. The pressure-transmitting medium is helium for the Ce_3Al metallic glass and silicon oil for α-Ce_3Al experiment.

Structural changes as a function of pressure were monitored by using synchrotron XRD with the wavelength of 0.3681(1) Å and a focused beam size of 15×15 μm^2. In situ high-pressure XRD experiments were performed at beamline 16ID-B of the High Pressure Collaborative Access Team, Advanced Photon Source (APS), Argonne National Laboratory. High-pressure Ce L_3-edge XAS experiments were carried out at beamline 20BM-B, APS. Samples are loaded in a Mao-type panoramic DAC with Be gasket and silicon oil as the pressure media. The DAC was tilted at 18° to minimize the absorption of Be gasket and diamond anvils in the beam path.

Ab initio theoretical calculations for the atomic radii and electronegativity of both localized and itinerant Ce in the fcc-Ce_3Al alloy were conducted. The total energy calculations were carried out within the framework of generalized gradient approximation (32) to density functional theory (33, 34) by using the projector augmented wave (PAW) method (35) as implemented in the Vienna Ab initio Simulation Package (36). The PAW potentials with the valence states $3s3p$ for Al, $5s5p5d6s$ for localized-f Ce, and $5s5p4f5d6s$ for delocalized-f Ce were used. All results reported here have been successfully tested for convergence with respect to cutoff energy and k-points. Ionic positions and cell parameters were relaxed with respect to minimum forces and stress by using conjugate-gradient algorithms.

ACKNOWLEDGMENTS. We thank Dr. C. L. Qin (Institute for Materials Research, Tohoku University, Sendai, Japan) for the starting material synthesis; Dr. M. J. Lipp for sharing Ce volume data; and Drs. R. E. Cohen, M. Guthrie, H. W. Sheng, and H. Z. Liu for helpful discussions. Use of the High Pressure Collaborative Access Team facility was supported by the Department of Energy–Basic Energy Sciences, Department of Energy–National Nuclear Security Administration (Carnegie/Department of Energy Alliance Center), National Science Foundation, Department of Defense–Tank-Automotive and Armaments Command, and the W. M. Keck Foundation. The Advanced Photon Source is supported by the Department of Energy– Basic Energy Sciences under Contract DE-AC02–06CH11357. Pacific Northwest Consortium Collaborative Access Team/X-ray Operations and Research facilities at the Advanced Photon Source, and research at these facilities, are supported by the U.S. Department of Energy–Basic Energy Sciences, a major facilities access grant from Natural Sciences and Engineering Research Council of Canada, University of Washington, Simon Fraser University, and the Advanced Photon Source. This work was supported by the Balzan Foundation, National Natural Science Foundation of China Grants 50425102, 50601021, 50701038, 60776014, 60876002, and 10804096, the Zhejiang University–Helmholtz Cooperation Fund, the Ministry of Education of China (Program for Changjiang Scholars, the Research Fund for the Doctoral Program of Higher Education from China Scholarship Council), the Department of Science and Technology of Zhejiang Province, and Zhejiang University. W.L., A.B., and R.A. are grateful to the Swedish Research Council for providing financial support, the Swedish National Infrastructure for Computing, and the Uppsala Multidisciplinary Center for Advanced Computational Science for providing computational resources.

1. Hume-Rothery W, Smallman RE, Haworth CW (1969) *Structure of Metals and Alloys* (Institute of Metals, London).
2. McMillan PF (2006) Chemistry at high pressure. *Chem Soc Rev* 35:855–857.
3. Atou T, Hasegawa M, Parker LJ, Badding JV (1996) Unusual chemical behavior for potassium under pressure: Silver-potassium compounds. *J Am Chem Soc* 118:12104–12108.
4. Parker LJ, Atou T, Badding JV (1996) Transition element-like chemistry for potassium under pressure. *Science* 273:95–97.
5. Tse JS, Frapper G, Ker A, Rousseau R, Klug DD (1999) Phase stability and electronic structure of K-Ag intermetallics at high pressure. *Phys Rev Lett* 82:4472–4475.
6. Dubrovinskaia N, *et al.* (2005) Beating the miscibility barrier between iron group elements and magnesium by high-pressure alloying. *Phys Rev Lett* 95:245502.
7. Johansson B, Abrikosov IA, Aldén M, Ruban AV, Skriver HL (1995) Calculated phase diagram for the γ-α transition in Ce. *Phys Rev Lett* 74:2335–2338.
8. Lavagna M, Lacroix C, Cyro M (1983) The γ-α transition in cerium compounds. *J Phys F* 13:1007–1015.
9. Vohra YK, Beaver SL, Akella J, Ruddle CA, Weir ST (1999) Ultrapressure equation of state of cerium metal to 208 GPa. *J Appl Phys* 85:2451–2453.
10. Bridgman PW (1927) *Proc Am Acad Arts Sci* 62:207–226.
11. Murani AP, Levett SJ, Taylor JW (2005) Magnetic form factor of α-Ce: Toward understanding the magnetism of cerium. *Phys Rev Lett* 95:256403.
12. Rueff JP, *et al.* (2006) Probing the γ-α transition in bulk Ce under pressure: A direct investigation by resonant inelastic X-ray scattering. *Phys Rev Lett* 96:237403.
13. Allen JW, Martin RM (1982) Kondo volume collapse and the $\gamma \rightarrow \alpha$ transition in cerium. *Phys Rev Lett* 49:1106–1110.
14. de'Medici L, Georges A, Kotliar G, Biermann S (2005) Mott transition and Kondo screening in f-electron metals. *Phys Rev Lett* 95:066402.
15. McMahan AK, Held K, Scalettar RT (2003) Thermodynamic and spectral properties of compressed Ce calculated using a combined local-density approximation and dynamical mean-field theory. *Phys Rev B* 67:075108.
16. Zölfl MB, Nekrasov IA, Pruschke T, Anisimov VI, Keller J (2001) Spectral and magnetic properties of α- and γ-Ce from dynamical mean-field theory and local density approximation. *Phys Rev Lett* 87:276403.
17. Gilman JJ (1980) Metallic glasses. *Science* 208:856–861.
18. Greer AL, Ma E (2007) Bulk metallic glasses: At the cutting edge of metals research. *MRS Bull* 32:611–615.
19. Sheng HW, *et al.* (2007) Polyamorphism in a metallic glass. *Nat Mat* 6:192–197.
20. Sheng HW, Luo WK, Alamgir FM, Bai JM, Ma E (2006) Atomic packing and short-to-medium range order in metallic glasses. *Nature* 439:419–425.
21. Zeng QS, *et al.* (2007) Anomalous compression behavior in lanthanum/cerium-based metallic glass under high pressure. *Proc Natl Aca Sci USA* 104:13565–13568.
22. Hemley RJ, Chen LC, Mao HK (1989) New transformations between crystalline and amorphous ice. *Nature* 338:638–640.
23. Liu H, *et al.* (2008) Anomalous high-pressure behavior of amorphous selenium from synchrotron X-ray diffraction and microtomography. *Proc Natl Acad Sci USA* 105:13229–13234.
24. Kim J-J, Choi Y, Suresh S, Argon AS (2002) Nanocrystallization during nanoindentation of a bulk amorphous metal alloy at room temperature. *Science* 295:654–657.
25. Sun L, *et al.* (2000) Reversible phase transition between amorphous and crystalline in $Zr_{41.2}Ti_{13.8}Cu_{12.5}Ni_{10}Be_{22.5}$ under high pressure at room temperature. *Appl Phys Lett* 76:2874–2876.
26. Chen YY, *et al.* (2000) Size-induced transition from magnetic ordering to Kondo behavior in (Ce,Al) compounds. *Phys Rev Lett* 84:4990–4993.
27. Lawson AC, Lawrence JM, Thompson JD, Williams A (1990) A Low temperature crystal structure of Ce_3Al. *Physica B* 163:587–590.
28. Lipp MJ, *et al.* (2008) Thermal signatures of the Kondo volume collapse in cerium. *Phys Rev Lett* 101:165703.
29. Olsen JS, Gerward L, Benedict U, Itié J-P (1985) The crystal structure and the equation of state of cerium metal in the pressure range 0–46 GPa. *Physica B* 133:129–137.
30. Singh AK, Liermann H-P, Akahama Y, Kawamura H (2007) Aluminum as a pressure-transmitting medium cum pressure standard for X-ray diffraction experiments to 200 GPa with diamond anvil cells. *J Appl Phys* 101:123526-1–123526-6.
31. Rueff J-P, *et al.* (2004) *f*-state occupancy at the γ-α phase transition of Ce-Th and Ce-Sc alloys. *Phys Rev Lett* 93:067402.
32. Perdew JP, Burke K, Ernzerhof M (1996) Generalized gradient approximation made simple. *Phys Rev Lett* 77:3865–3868.
33. Hohenberg P, Kohn W (1964) Inhomogeneous electron gas. *Phys Rev* 136:B864–B871.
34. Kohn W, Sham LJ (1965) Self-consistent equations including exchange and correlation effects. *Phys Rev* 140:A1133–A1138.
35. Blöchl PE (1994) Projector augmented-wave method. *Phys Rev B* 50:17953–17979.
36. Kresse G, Furthmüller J (1996) Efficient iteractive schemes for ab initio total-energy calculations using a plane-wave basis set. *Phys Rev B* 54:11169–11186.